

Characterization of optical fiber at cryogenic temperatures

Adam J. Christiansen^{*a,b}, Matthew Popelka^c, Brad G. Gom^{a,b}, David A. Naylor^a,
and Andrei A. Stolov^c

^aUniversity of Lethbridge, 4401 University Dr W, Lethbridge, AB T1K 3M4, Canada

^bBlue Sky Spectroscopy Inc., Lethbridge, AB T1J 0N9, Canada

^cOFS, 55 Darling Dr, Avon, CT 06001, USA

ABSTRACT

Optical fibers are commonly used for data transmission and sensing in industrial, geophysical, and aerospace markets, where they may be employed in high vacuum and cryogenic environments. The performance and integrity of optical fibers and their coatings is well understood over temperatures of -40 to 300 °C and pressures up to 100 atm, but their characteristics at cryogenic temperatures under high vacuum remain relatively unexplored. This study investigates the optical and mechanical reliability of selected fibers operating at cryogenic temperatures. The fiber samples under investigation were prepared with either an acrylate or polyimide coating. Several properties of the fibers were assessed, including optical loss, mechanical strength, and coating integrity. Optical loss was monitored continuously over a single temperature cycle from ~ 300 K to 4 K and back. Additional samples were subjected to either one or three temperature cycles and held at 4 K for extended periods. Mechanical strength of the thermally cycled fibers was determined via a 2-point bend method, and the coating material was characterized using Fourier transform infrared spectroscopy and thermogravimetric analysis.

Keywords: Optical fiber, cryogenic, polyimide, acrylate, coating

1. INTRODUCTION

Optical fibers have favorable properties such as immunity from electromagnetic disturbances, chemical inertness, and compact packaging, which make them useful in a variety of applications. In addition to their extensive use in telecommunications, optical fibers are widely and successfully used for laser generation and numerous types of sensing.¹ The waveguide of most optical fibers is made of pure or doped silica, which enables outstanding light transmission in the near infrared region. For mechanical protection, the silica waveguide is coated with a polymer material, like an acrylate, silicone, or polyimide. An application requiring exposure to harsh conditions may be challenging for the fiber, as severe environments, such as water or crude oil, for instance, can lead to degradation or dissolution of the polymer coating; resulting in weakening or even fracture of the fiber.² A mismatch of the coefficients of thermal expansion (CTE) might create microbends in the waveguide and possible defects in the coating, such as cracks or delaminations.³ These two effects may lead to added optical loss.⁴

Within the last few decades, much attention has been given to high temperature applications of optical fibers, primarily because of their usage in the oil industry.^{5,6} Low temperature applications are less explored, specifically those involving cryogenic environments. At such temperatures, fibers are primarily used for probing and sensing, and the need to understand their performance and reliability is essential. Fiber Bragg grating techniques are commonplace for discrete point sensors; while Rayleigh, Raman, and Brillouin scattering are utilized in distributed sensing. These sensors can monitor a variety of parameters such as temperature,⁷⁻¹¹ strain in superconducting magnets,¹²⁻¹⁴ and liquid levels for liquefied natural gas and hydrogen.¹⁵ Early testing of optical fibers at 77 K found them suitable for use in infrared instrumentation for space-based applications,¹⁶ and fibers are currently utilized under cryogenic conditions in quantum computing.¹⁷

While direct exposure of fibers to liquid nitrogen (77 K) has been examined,^{18,19} the effects at liquid helium temperatures (4 K) are largely unexplored. Future far-infrared space astronomy applications will utilize fibers

Further author information: (Send correspondence to A.J.C.)

A.J.C.: E-mail: adam.christiansen@uleth.ca

cooled to 4 K, such as those discussed in prior work,^{20–23} and the exploration of cryogenic applications for a multi-axis range-resolved laser interferometer presented in a companion paper at this conference (Christiansen et al., *ibid.* 12428–53). For space-based applications, reliability takes a special precedence over performance, as small increases in attenuation are generally tolerable, but a failure caused by damage to a fiber is irrecoverable. Establishing the reliability of optical fibers at cryogenic temperatures is essential, as the fiber must not only survive in space for the duration of the mission, but must also survive mandatory testing and verification processes during which the instrumentation temperature cycled many times. In the verification phase of a project, one must have confidence that the selected fiber will not sustain damage that will lead to a failure once deployed.

This paper explores the optical and mechanical reliability of selected fibers when subjected to high vacuum environments with temperatures of ~ 4 K. Several properties of acrylate and polyimide coated fibers were assessed, including optical loss, mechanical strength, and coating integrity. Optical loss was monitored continuously over a single temperature cycle from room temperature to ~ 4 K and back. Additional samples were subjected to either one or three temperature cycles and held at ~ 4 K for extended periods. Mechanical strength of the temperature cycled fibers was determined via a 2-point bend method, and the coating material was characterized using Fourier transform infrared spectroscopy and thermogravimetric analysis.

2. EXPERIMENTAL DESIGN

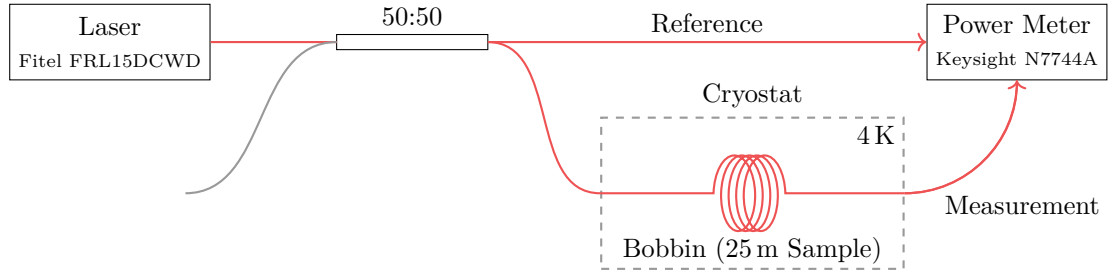
Several pairs of fibers were prepared for cryogenic temperature cycling, consisting of one acrylate and one polyimide coated fiber. All fibers were drawn from silica preforms and coated during draw with either a dual acrylate or polyimide. The glass cladding diameter was $125\ \mu\text{m}$ with a single-mode waveguide design type G.652 having a core diameter of $\sim 8.2\ \mu\text{m}$.²⁴ Coating diameters were in the range of 240 to $245\ \mu\text{m}$ and 150 to $155\ \mu\text{m}$ for acrylate and polyimide, respectively. Fibers were proof tested at 100 kpsi for acrylate and 200 kpsi for polyimide coated samples. Characterization includes cryogenic optical loss monitoring, mechanical strength testing, and coating analysis.

2.1 Cryogenic Optical Loss Monitoring

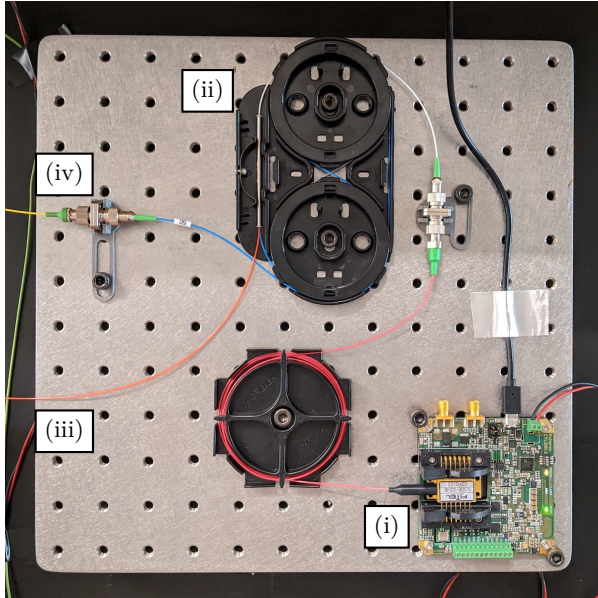
A pair of 25 m FC/APC terminated fibers was prepared for optical loss monitoring. The optical signal was monitored continuously for three temperature cycles from ambient to ~ 4 K and back, with a cryogenic dwell time of 3 hours. A schematic of the experimental configuration is shown in [Figure 1a](#) and pictured in [Figures 1b](#) and [1c](#). A Fitel FRL15DCWD 1550 nm DFB laser diode is driven by a Koheron CTL200 butterfly laser controller for CW operation with an optical power output of 37 mW. The laser light is split by a 50:50 coupler: one signal serves as a reference to correct for long-term fluctuations in laser power, and the other signal passed through the fiber under test in the cryostat, pictured in [Figure 1b](#). Both signals are sampled at 1 Hz using a Keysight N7744A power meter. At the test wavelength of 1550 nm, the G.652 fiber design is single-mode.²⁴

[Figure 1c](#) shows the apparatus installed in the cryostat. A custom aluminum bobbin was constructed with a 120 mm inner diameter, better shown in [Figure 1d](#) with lengths acrylate and polyimide fibers installed. A temperature sensor attached to the bobbin monitors its temperature; and it is assumed that the bobbin and fibers are in thermal equilibrium. The bobbin is secured to the 4 K plate of the cryostat by an aluminum bar bolted through the center, as shown in [Figures 1c](#) and [1e](#). The bar is preferred over through-holes for greater mounting flexibility and to better distribute the mounting force over the contact area between the bobbin and the 4 K plate to optimize thermal conduction.

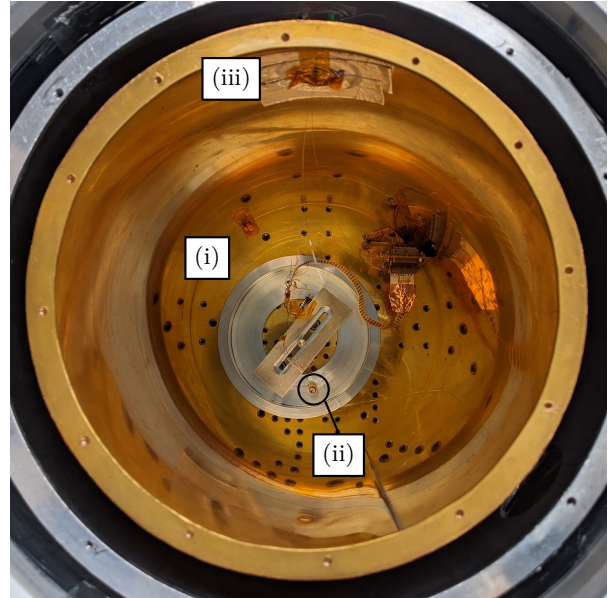
When wrapped around the bobbin, 50 cm of fiber was left at either end so that the FC/APC terminated ends could reach the hermetic fiber feedthrough on the outer cryostat wall when the bobbin is mounted to the 4 K plate, leaving 24 m of fiber in contact with the bobbin. [Figure 1c](#) shows the configuration of the bobbin and fibers under test in the cryostat. Each fiber was cycled three times while the change in transmission through the fiber was monitored. The cryostat was kept under vacuum for the three cycles of each sample.



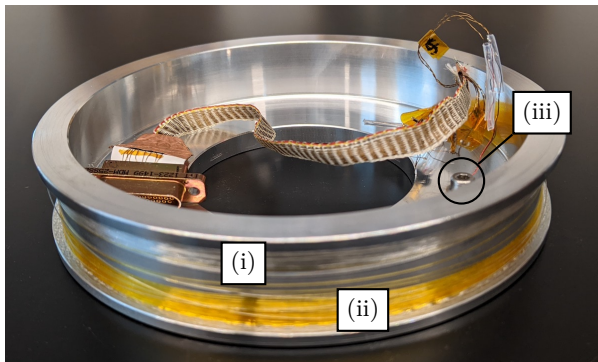
(a) Schematic of the cryogenic optical loss monitoring experiment. In the cryostat, the fiber is wrapped several times around a bobbin mounted to the 4 K plate.



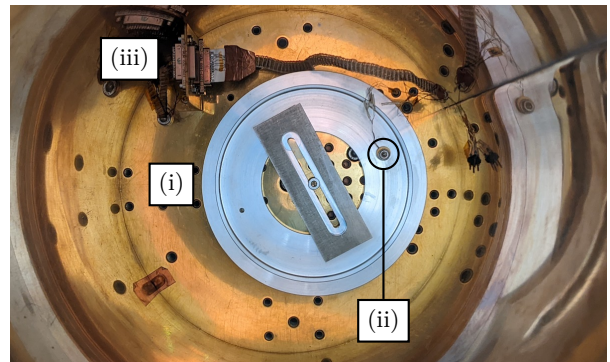
(b) Light from the fiber-coupled laser (i) is guided to a 50:50 coupler (ii). The first coupler output is the reference signal (iii), and the second output (iv) passes through the fiber under test in the cryostat, shown to the right in (c).



(c) The aluminum bobbin holding the 25 m test fiber is secured to the 4 K plate of a cryostat by an aluminum bar (i); a temperature sensor (ii) is bolted to the bobbin. The fiber ends pass through a hole in the shielding (iii) to a hermetic fiber feedthrough.



(d) 25 m lengths of acrylate coated fiber (i) and polyimide fiber (ii) wrapped around the aluminum bobbin. A temperature sensor (iii) is secured to the bobbin before installation in the cryostat.



(e) The aluminum bobbin (i) secured to the 4 K plate of the cryostat for cycling unterminated fibers. The temperature sensor (ii) is connected to the cryostat electrical harness (iii) (which is also visible in (c)).

Figure 1: Experimental configurations for cryogenic optical loss monitoring are shown in (a), (b), and (c); configurations for mechanical strength and coating characterization are shown in (d) and (e).

2.2 Mechanical Strength and Coating Characterization

Three pairs of unterminated 20 m fibers were prepared for mechanical strength and coating characterization. Two pairs were temperature cycled, while the third pair served as an as-drawn unaged control fiber sample. Of the two cycled pairs, one underwent a single temperature cycle, while the other was cycled three times. Both samples in a pair were cycled simultaneously on the same bobbin to guarantee that they both undergo the same aging process. Figure 1d shows an acrylate-polyimide pair on the bobbin before installation in the cryostat. Each temperature cycle had a minimum dwell time of 12 hours at ~ 4 K. For the pair cycled three times, the cryostat was not opened between cycles, and the samples were kept under vacuum for the entire duration.

After low temperature and high vacuum exposure, the fiber coating appearance was inspected for possible cracks using a Nikon Optiphot optical microscope combined with a CCD camera. Mechanical strength of the unaged and aged fiber samples was determined using a 2-point bend technique (Fiber Sigma Instruments) at strain rates of 0.08%/min, 0.57%/min, 4%/min, and 28%/min. The fibers were preconditioned at $23 \pm 2^\circ\text{C}$ and $50 \pm 5\%$ RH for at least 24 hours before testing. For each fiber and aging condition, 5 to 20 strength measurements were made to ensure statistical reliability of gathered and analyzed data.

The coating material was characterized via infrared micro attenuated total reflection spectroscopy (micro-ATR). The spectra were collected using a Thermo-Fischer iS50 Fourier transform infrared spectrometer equipped with a LN_2 cooled detector and internal reflection elements of ZnSe and Ge, and averaged over 64 scans. Thermogravimetric analysis (TGA) was performed using a TA Instruments TGA Q500 over a temperature range from ambient to 800°C . The tested samples were short pieces of fiber with masses in the range of 10 to 20 mg. The samples were placed in a platinum pan inside of a chamber purged with dry air at a flow rate of $60\text{ cm}^3/\text{min}$. Rate for mass loss was followed dynamically, for which the samples were ramped to a temperature of 650°C at a rate of $10^\circ\text{C}/\text{min}$, and then to a temperature of 800°C at $20^\circ\text{C}/\text{min}$.

3. RESULTS

3.1 Optical Loss

Each fiber was cycled three times while the change in transmission through the fiber was monitored. The measurement and reference powers are discrete time series, $P_m[n]$ and $P_r[n]$, respectively. A corrected power ratio is given by $p[n] = P_m[n]/P_r[n]$, which accounts for fluctuations in the laser output power, allowing the

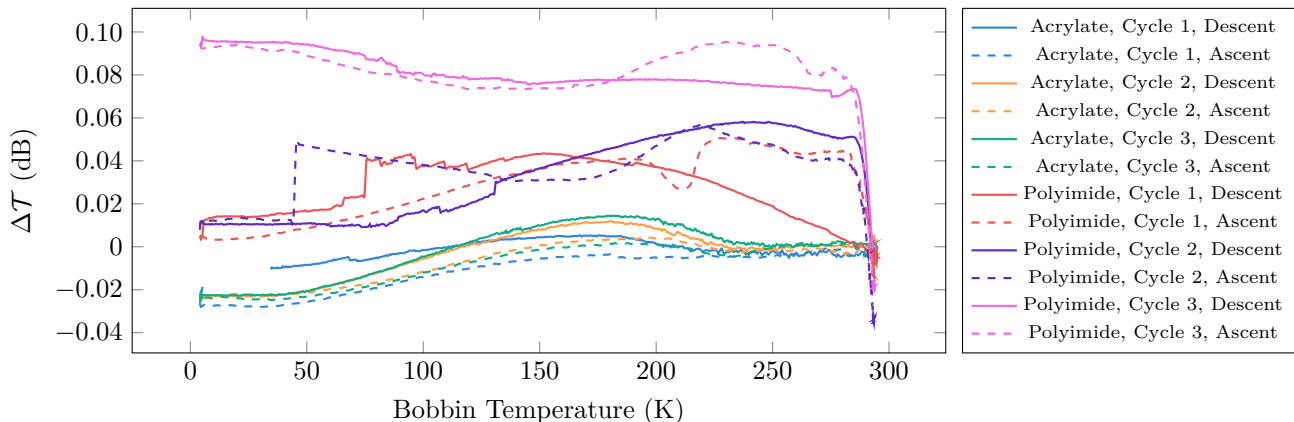


Figure 2: The change in transmission for both fiber samples, split into the descent and ascent curves. The acrylate coated fiber is consistent and shows a tendency for loss when cooled; the polyimide coated fiber is inconsistent but shows a general transmission increase when cooled. In the *Acrylate, Cycle 1, Descent* curve, the temperature sensor reading was lost in the 5 to 34 K range. The measurement uncertainty is 10^{-6} dB, indicating that the small observed jumps are physical and not due to measurement errors. For reference, a change of 0.1 dB is approximately 2.3%.

change in transmission, $\Delta\mathcal{T}[n]$, in dB, to be computed by

$$\Delta\mathcal{T}[n] = 10 \log_{10} \frac{p[n]}{p[0]}. \quad (1)$$

As $\Delta\mathcal{T}$ is the change in transmission, not attenuation, an increase $\Delta\mathcal{T}$ indicates that more optical power is transmitted through the fiber. Using Equation (1), Figure 2 plots the change in transmission as a function of the bobbin temperature, with the solid and dashed curves representing the descent and ascent phases, respectively.

The acrylate coated fiber demonstrates repeatable behavior among the three temperature cycles. At the lowest temperature, an optical loss of -0.023 to -0.027 dB is observed in comparison to room temperature, however, in the range of 120 to 220 K, the transmission is seen to increase reaching a maximum of 0.014 dB near 180 K. The curves exhibit a non-linear temperature dependence, which is attributed to the counteractive effects of scattering and microbends along the fiber. For modern silica-based fibers, the attenuation within 1300 to 1600 nm range is dominated by Rayleigh scattering caused by intrinsic nanoscopic density fluctuations in the glass.⁴ Lowering the temperature reduces the frequency of thermally activated density fluctuations, which may reduce the Rayleigh scattering and improve the transmission. When the fiber is cooled, differences in coefficients of thermal expansion (CTE) between the silica glass and the polymer coating material impose an axial compressive stress on the fiber, leading to microbends — small deflections of the fiber axis that are random in amplitude and distribution along the fiber length that are known to increase optical loss.⁴ Reduced Rayleigh scattering and development of microbends counteract each other at low temperatures, resulting in the observed transmission profile.

Unlike the acrylate coating, the polyimide does not show consistency over each cycle. In Figure 2, several unexpected step changes are observed, which are random in direction. For instance, the cycle 1 descent exhibits a sudden loss of 0.016 dB near 75 K, while there is a sudden 0.035 dB gain near 45 K in the cycle 2 ascent. Furthermore, cycle 3 differs dramatically from the other polyimide curves, and shows an average ~ 0.04 dB transmission increase over cycles 1 and 2. When cooled in cycle 3, the transmission is better than ambient for the entire descent, and most of the ascent until about 290 K. In the region of 4.2 to 40 K, cycle 3 exhibits a ~ 0.095 dB improvement with respect to room temperature. All curves for acrylate coatings consistently return to ± 0.003 dB after each ascent, while the curves for polyimide coatings yield greater variation, and return to -0.036 to -0.013 dB.

The polyimide coating thickness is much smaller than that of the acrylate (which are 15 μm and 60 μm , respectively), suggesting the polyimide coated fiber will experience fewer effects from the induced axial stress on the fiber — however, a thin coating makes the fiber more sensitive to extreme temperature gradients along

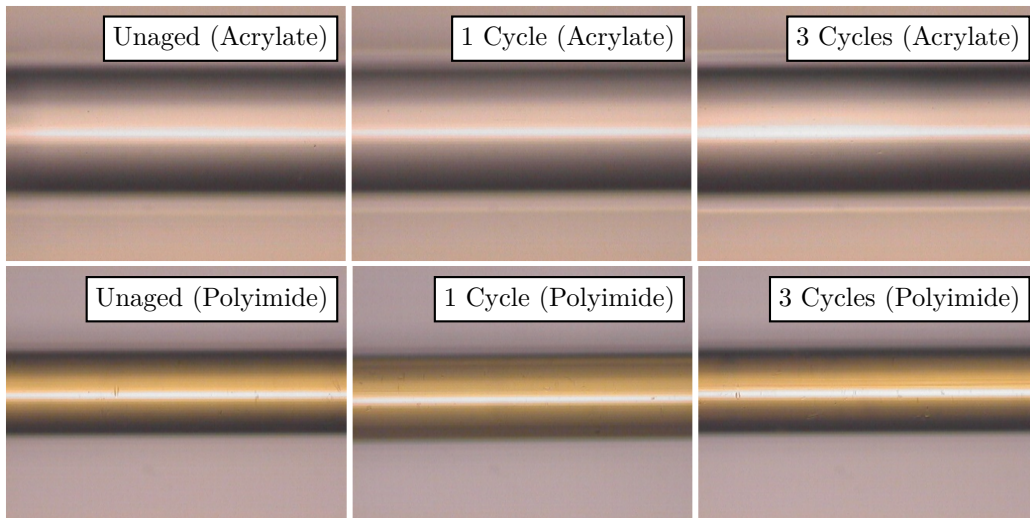


Figure 3: Optical images of unaged and temperature cycled acrylate and polyimide coated fibers.

its length. The 50 cm of fiber at each end of the sample extending from the bobbin to the fiber feedthrough on the cryostat wall will have a ~ 300 K temperature gradient. Since the observed sudden changes in Figure 2 are not reproducible, they are attributed to the development of local coating defects, like cracks and coating-glass delaminations. These could be either isolated to specific locations like the termination end of the sample, or throughout the whole length under test. The temperature induced stress on the polyimide coating, σ , can be estimated as

$$\sigma = E_{\text{PI}}(\alpha_{\text{PI}} - \alpha_{\text{SiO}_2})\Delta T, \quad (2)$$

where E_{PI} is the coating Young’s modulus, α_{PI} and α_{SiO_2} are CTEs of the coating and glass, respectively, and ΔT is the temperature variation. The room temperature Young’s modulus of the polyimide material is about 2 GPa and its CTE is about 40 ppm/K; the CTE of pure silica is much lower at 0.55 ppm/K. Assuming the largest temperature variation of 300 K, Equation (2) estimates an induced tensile stress of ~ 24 MPa. This should be compared with the strength of polyimide, which at room temperature is about 130 MPa, and could be assumed the same or higher at cryogenic temperatures. The induced stress is ~ 5 times lower than the strength of polyimide, indicating that systematic coating cracking is unlikely. Although there is a lack of clear experimental evidence for the coating-glass delaminations, this mechanism seems to be a more reasonable explanation for the transmission behavior shown in Figure 2. Absence of cracking is indirectly supported by the room temperature optical microscopy images in Figure 3, showing the coating of unaged and temperature cycled fibers. Several centimeters of each fiber were explored using a microscope, and neither the acrylate nor the polyimide coatings exhibited cracking.

3.2 Mechanical Strength

Potential microcracking and coating-glass delaminations can be detected by measuring mechanical strength and fatigue parameters of optical fiber via 2-point bend testing. The length involved in the actual bend is very short, and that is why the 2-point bend approach characterizes the fiber strength at a “microscopic scale”.²⁵ The obtained strength results characterize solely the coating-glass system while possibly ignoring infrequent defects, which normally are removed by proof testing. Figures 4a and 4b show the data collected at 4%/min strain rate. From Table 1, median strength magnitudes were found to be ~ 5.2 GPa for the acrylate and ~ 5.6 GPa for the polyimide coated samples. The fracture stress distributions can be characterized by Weibull slopes (or m -values);²⁶ narrow distributions correspond to high Weibull slopes. In all studied samples, the Weibull slopes exceed 30, indicating the absence of “weak spots” along the fibers and that the excursions to ~ 4 K did not result in strength reduction of the fibers.

From the 2-point bend data collected at different strain rates, as shown in Figure 4c, stress corrosion resistance parameters, n_d , were determined. The n_d values characterize how long the fiber will survive at applied tensile

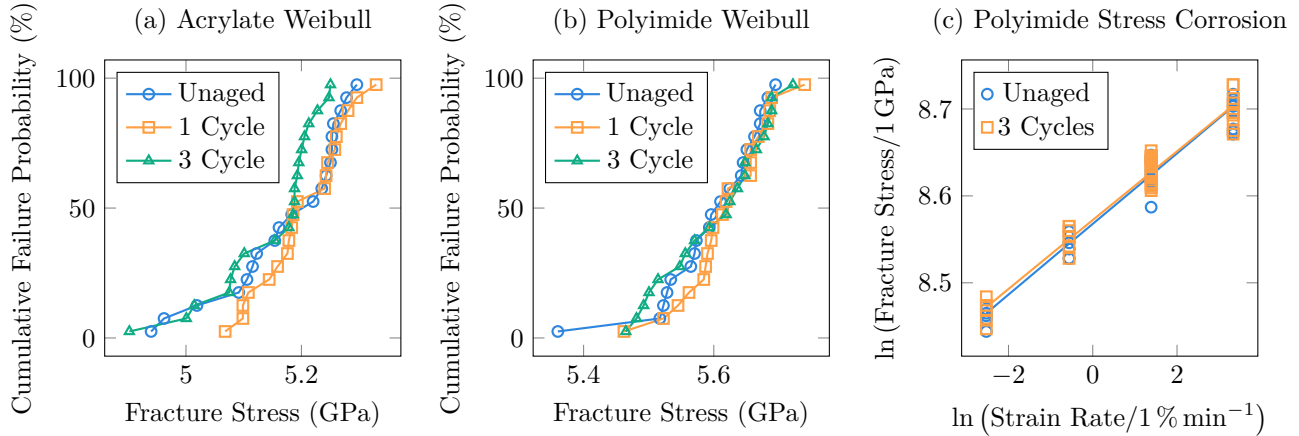


Figure 4: Weibull plots (4%/min) showing mechanical strength of unaged and temperature cycled acrylate and polyimide coated fiber samples are shown in (a) and (b), respectively; stress corrosion data for polyimide fiber is plotted in (c).

Table 1: Mechanical strength of the fiber samples.

Coating	Acrylate			Polyimide		
	Unaged	1 Cycle	3 Cycles	Unaged	1 Cycle	3 Cycles
Strength (GPa)	5.17	5.20	5.14	5.60	5.62	5.60
Weibull Slope	59	85	67	85	105	84
n_d	19.8 ± 1.1	19.7 ± 0.6	19.5 ± 1.2	23.6 ± 1.0	23.3 ± 0.8	24.2 ± 1.2

or bend stress, and per the industry standards, such values must be ≥ 18 . In all cases for acrylate and polyimide coatings, Table 1 shows that n_d not only exceeds 18, but also that low temperature excursions did not cause reduction of n_d .

The absence of the strength degradation may be interpreted as an absence of embrittlement, cracks, and delaminations in both fibers. Alternatively, if the coating defects were in effect at low temperatures, their consequences must be recovered after bringing the fibers back to ambient conditions, thus, potential delaminations between the polyimide and glass are not causing catastrophic effects.

3.3 Coating Characterization

Possible alterations in the coating chemistry were analyzed by FTIR spectroscopy. Figures 5a and 5b show the spectra collected from the secondary acrylate and polyimide coatings, respectively. The provided spectral range

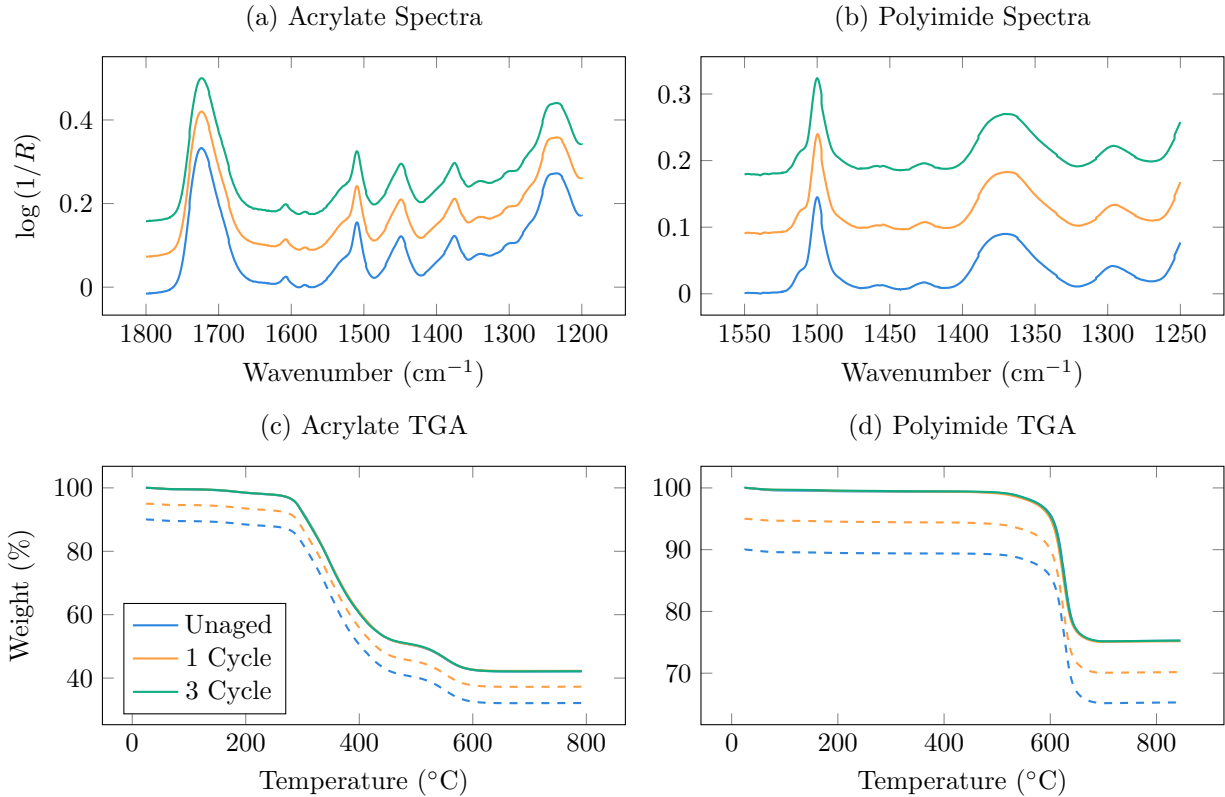


Figure 5: FTIR spectra of the secondary acrylate (a) and polyimide coatings (b) collected from the unaged and temperature cycled fibers. Spectra are offset, and only a subset of wavenumbers are shown. Thermogravimetry (TGA) curves are plotted for acrylate (c) and polyimide (d) coated fiber samples. In (c) and (d), all three solid curves are overplot to show their consistency, while for visibility, the blue and orange dashed curves show the *Unaged* and *1 Cycle* curves offset, respectively. The legend in the bottom left applies to all four plots.

includes peaks of the carbonyl (1730 cm^{-1}), urethane (1530 cm^{-1}), and acrylate (1410 cm^{-1}) groups. Spectra for the three acrylate and polyimide samples are identical over all three test conditions and show no change of the peak intensities across the wavenumbers for each coating type. The spectra collected for the primary acrylate and polyimide coatings showed similar results. Specifically for the polyimide coating, there is an imide peak at 1360 cm^{-1} in Figure 5b, which describes imidization of the coating after cure. Identical spectra for all three test conditions indicates there were no changes in the coating materials at the molecular level.

High vacuum exposure during temperature cycling might result in loss of volatile components of the coatings. Potential loss of volatiles was analyzed via thermogravimetry (TGA), where the masses of the coated fiber samples were measured while heating at a constant rate. A loss of volatiles would shift the mass-temperature curves, which are superposed in Figures 5c and 5d for acrylate and polyimide, respectively. As no difference is observed for either coating, the loss of volatiles, if any, was insignificant.

4. CONCLUSIONS

Optical fiber samples with either a dual acrylate or polyimide coating have been subjected to cryogenic temperatures of $\sim 4\text{ K}$ under high vacuum. Optical loss was monitored for three temperature cycles from ambient to $\sim 4\text{ K}$ and back. The acrylate coated fiber showed repeatable results while the polyimide coated fiber exhibited significant variations across all cycles. The latter phenomenon is tentatively attributed to coating-glass delaminations and effects of the extreme temperature gradient between the 4 K plate of the cryostat and fiber feedthrough on the vacuum chamber, but warrants further exploration. Analysis of the unaged and cycled fibers via optical microscopy showed no cracking in either coating, and 2-point bend testing revealed no loss in strength or evidence of fatigue in fibers with either coating type. Coating material characterization via FTIR and TGA also showed no changes across the temperature cycles. These results give confidence in using acrylate coated optical fiber for cryogenic applications, while more cryogenic testing of polyimide coated fibers would be useful to improve the statistics in the observed transmission increase.

ACKNOWLEDGMENTS

This research is supported by: Alberta Innovates, Blue Sky Spectroscopy Inc., Canada Foundation for Innovation, Canadian Microelectronics Corporation, Canadian Space Agency, NSERC, NTCO CREATE, OFS, and the University of Lethbridge.

REFERENCES

- [1] Del Villar, I. and Matias, I. R., [*Optical Fibre Sensors: Fundamentals for Development of Optimized Devices*], John Wiley & Sons (2020).
- [2] Stolov, A. A., Simoff, D. A., Li, J., Hokansson, A. S., and Hines, M. J., "Behavior of specialty optical fibers in crude oil environment," *Journal of Lightwave Technology* **38**(14), 3759–3768 (2020).
- [3] Stolov, A. A. and Simoff, D. A., "Thermal stability of optical fiber coatings: comparison of experimental thermogravimetric approaches," *Journal of Thermal Analysis and Calorimetry* **146**(4), 1773–1789 (2021).
- [4] Lingle, R., Peckham, D., McCurdy, A., and Kim, J., "Light-guiding fundamentals and fiber design," *Specialty Optical Fibers Handbook*, 19–68 (2007).
- [5] Reinsch, T. and Hennings, J., "Temperature-dependent characterization of optical fibres for distributed temperature sensing in hot geothermal wells," *Measurement Science and Technology* **21**(9), 094022 (2010).
- [6] Stolov, A. A., "Aging of optical fibers in aggressive environments: Mimicking downhole and undersea applications," in [*Proc. 67th Int. Wire Cable Symp.*], 15–1 (2018).
- [7] De Miguel-Soto, V., Leandro, D., Lopez-Aldaba, A., Beato-López, J. J., Pérez-Landazábal, J. I., Auguste, J.-L., Jamier, R., Roy, P., and Lopez-Amo, M., "Study of optical fiber sensors for cryogenic temperature measurements," *Sensors* **17**(12), 2773 (2017).
- [8] Lu, X., Soto, M. A., and Thévenaz, L., "Impact of the fiber coating on the temperature response of distributed optical fiber sensors at cryogenic ranges," *Journal of Lightwave Technology* **36**(4), 961–967 (2017).

- [9] Yue, Y., Chen, G., Long, J., Ren, L., Zhou, K., Li, X., Xu, Y., and Tang, Y., “Characterization of a Raman-based distributed fiber optical temperature sensor in liquid nitrogen,” *Superconductivity* **4**, 100028 (2022).
- [10] Swinehart, P., Maklad, M., and Courts, S., “Cryogenic fiber optic sensors based on fiber Bragg gratings,” in [*AIP Conference Proceedings*], **985**(1), 940–946, American Institute of Physics (2008).
- [11] Wu, M.-C., Pater, R. H., and DeHaven, S. L., “Effects of coating and diametric load on fiber Bragg gratings as cryogenic temperature sensors,” in [*Smart Sensor Phenomena, Technology, Networks, and Systems 2008*], **6933**, 28–37, SPIE (2008).
- [12] Chiuchiolo, A., Bajas, H., Bajko, M., Castaldo, B., Consales, M., Cusano, A., Giordano, M., Giloux, C., Pérez, J., Sansone, L., et al., “Cryogenic test facility instrumentation with fiber optic and fiber optic sensors for testing superconducting accelerator magnets,” in [*IOP Conference Series: Materials Science and Engineering*], **278**(1), 012082, IOP Publishing (2017).
- [13] Yang, T., Wang, Y., and Wang, X., “High-precision calibration for strain and temperature sensitivities of Rayleigh-scattering-based DOFS at cryogenic temperatures,” *Cryogenics* **124**, 103481 (2022).
- [14] Marcon, L., Chiuchiolo, A., Castaldo, B., Bajas, H., Galtarossa, A., Bajko, M., and Palmieri, L., “The characterization of optical fibers for distributed cryogenic temperature monitoring,” *Sensors* **22**(11), 4009 (2022).
- [15] Chen, T., Wang, Q., Chen, R., Zhang, B., Lin, Y., and Chen, K. P., “Distributed liquid level sensors using self-heated optical fibers for cryogenic liquid management,” *Applied Optics* **51**(26), 6282–6289 (2012).
- [16] Lee, D., Haynes, R., and Skeen, D., “Properties of optical fibres at cryogenic temperatures,” *Monthly Notices of the Royal Astronomical Society* **326**(2), 774–780 (2001).
- [17] Lecocq, F., Quinlan, F., Cicak, K., Aumentado, J., Diddams, S., and Teufel, J., “Control and readout of a superconducting qubit using a photonic link,” *Nature* **591**(7851), 575–579 (2021).
- [18] Lindholm, E. A., Stolov, A. A., Dyer, R. S., Slyman, B., and Burgess, D., “Reliability of optical fibers in a cryogenic environment,” in [*Fiber Optic Sensors and Applications VI*], **7316**, 258–263, SPIE (2009).
- [19] Stolov, A. A., Hokansson, A. S., Dyer, R. S., Marceau, K. L., Slyman, B. E., Cote, D. J., Li, J., and Ciardiello, C. R., “Effects of low temperature and hot steam on reliability of specialty optical fibers designed for avionics applications,” in [*2013 IEEE Avionics, Fiber-Optics and Photonics Technology Conference (AVFOP)*], 29–30, IEEE (2013).
- [20] Christiansen, A. J., Naylor, D. A., Anderson, A. M., and Gom, B. G., “A cryogenic fmcw range-resolved laser interferometer: challenges and applications,” *Photonic Instrumentation Engineering IX* **12008**, 25–38 (2022).
- [21] Veenendaal, I., Naylor, D., Gom, B., Christiansen, A., Jellema, W., Feenstra, C., Ridder, M., Eggens, M., and Ade, P., “An angle-scanned cryogenic Fabry–Pérot interferometer for far-infrared astronomy,” *Review of Scientific Instruments* **91**(8), 083108 (2020).
- [22] Christiansen, A. J., Naylor, D. A., Veenendaal, I. T., and Gom, B. G., “A frequency-modulated laser interferometer for nanometer-scale position sensing at cryogenic temperatures,” in [*Photonic Instrumentation Engineering VI*], **10925**, 228–239, SPIE (2019).
- [23] Naylor, D., Veenendaal, I., Gom, B., and Christiansen, A., “A fiber-fed laser interferometer for optical metrology at cryogenic temperatures,” in [*Photonic Instrumentation Engineering V*], **10539**, 171–182, SPIE (2018).
- [24] International Telecommunication Union, *G.652: Characteristics of a single-mode optical fibre and cable* (2016).
- [25] Matthewson, M. J., Kurkjian, C. R., and Gulati, S. T., “Strength measurement of optical fibers by bending,” *Journal of the American Ceramic Society* **69**(11), 815–821 (1986).
- [26] Kurkjian, C. R. and Matthewson, M. J., “Mechanical strength and reliability of glass fibers,” *Specialty Optical Fibers Handbook*, 735–781 (2007).